energies

MDPI

Article

Analysis of a Lab-Scale Heat Transformation Demonstrator Based on a Gas–Solid Reaction †

Jana Stengler *, Julius Weiss and Marc Linder

German Aerospace Center (DLR), Institute of Engineering Thermodynamics, 70569 Stuttgart, Germany; julius.weiss@ise.fraunhofer.de (J.W.); marc.linder@dlr.de (M.L.)

* Correspondence: jana.stengler@dlr.de; Tel.: +49-711-6862-8238

† The original paper was presented in: Stengler, J., Fischer, E., Weiss, J., Linder, M. Experimental Results of a 1 kW Heat Transformation Demonstrator based on a Gas–Solid Reaction. Riehl, R., Preißinger, M., Eames, I., Tierney, M., Eds. In Proceedings of the Heat Powered Cycles Conference 2018, Bayreuth, Germany, 16–19 September 2018. ISBN: 978-0-9563329-6-7.

Received: 27 April 2019; Accepted: 5 June 2019; Published: 12 June 2019

Abstract: Heat transformation based on reversible chemical reactions has gained significant interest due to the high achievable output temperatures. This specific type of chemical heat pump uses a reversible gas–solid reaction, with the back and forward reactions taking place at different temperatures: by running the exothermic discharge reaction at a higher temperature than the endothermic charge reaction, the released heat is thermally upgraded. In this work, we report on the experimental investigation of the hydration reaction of strontium bromide ($SrBr_2$) with regard to its use for heat transformation in the temperature range from 180 °C to 250 °C on a 1 kg scale. The reaction temperature is set by adjusting the pressure of the gaseous reactant. In previous experimental studies, we found the macroscopic and microscopic properties of the solid bulk phase to be subject to considerable changes due to the chemical reaction-. In order to better understand how this affects the thermal discharge performance of a thermochemical reactor, we combine our experimental work with a modelling approach. From the results of the presented studies, we derive design rules and operating parameters for a thermochemical storage module based on $SrBr_2$.

Keywords: heat transformation; thermochemical reaction; chemical heat pump; thermal upgrade; gas–solid reaction

1. Introduction

Thermochemical reactions, for example reversible reactions between a gas and a solid, have been widely discussed in literature in the context of thermal energy storage. Compared to latent or sensible energy storage technologies, thermochemical systems offer significantly higher energy storage densities [1]. Another key feature of thermochemical energy storage is the possibility to control the charge and discharge temperatures by adjusting the concentration of the reactants: if the gas pressure is increased in a gas–solid reaction system, the reaction temperature rises. This effect can be used to transform thermal energy from a lower temperature level to a higher temperature level, the so-called heat transformation or chemical heat pump [2,3]. Different thermodynamic heat transformation and chemical heat pump processes have been discussed in the literature, and a number of studies have been published that clearly highlight the potential of heat transformers for the reduction of low-enthalpy waste heat in industrial processes [4,5]. Although there are several lab-scale setups proposed with different gas–solid working pairs, no technical implementation of a thermochemical heat transformer on an industrial scale has been reported [6–8]. Regarding suitable gas–solid reactive couples, there is a broad spectrum of chemical reactions discussed, e.g., ammonia-, hydrogen- or steam-based working pairs, covering a wide range of operating temperatures [9].

The basic concept of heat transformation generally requires three temperature levels and two pressure stages (see Figure 1a, with water vapor being the gaseous reactant). For providing the reaction enthalpy ($\Delta_R H$) of the endothermic reaction as well as for supplying the evaporation enthalpy of the gaseous component ($\Delta_V H$), waste heat at a temperature of T_{waste} is used. During the charging process, the emerging vapor is condensed at ambient temperature ($T_{ambient}$). In our work, we follow a different approach to achieve thermal upgrade at a higher absolute temperature level. As depicted in Figure 1b, the heat transformation process described in this work requires four temperature stages: the two upper ones are related to the later application process, and the two lower ones are used for thermal compression of the gaseous reactant. The lowest temperature level (condensation at ambient temperature $T_{ambient}$) is needed for vapor removal from the reaction chamber in order for the endothermic reaction to reach complete turnover at a low pressure (p_{low}). Hence, the chemical reaction takes place at a low reaction temperature ($T_{low\ val.}$), and the thermochemical storage is charged by low-value process heat. During the exothermic discharging process, low-temperature waste heat is used for providing steam at a higher pressure (p_{high}) for running the chemical reaction. The available waste heat temperature defines the vapor pressure and, thus, determines the maximum thermal upgrade of the released high-value process heat.

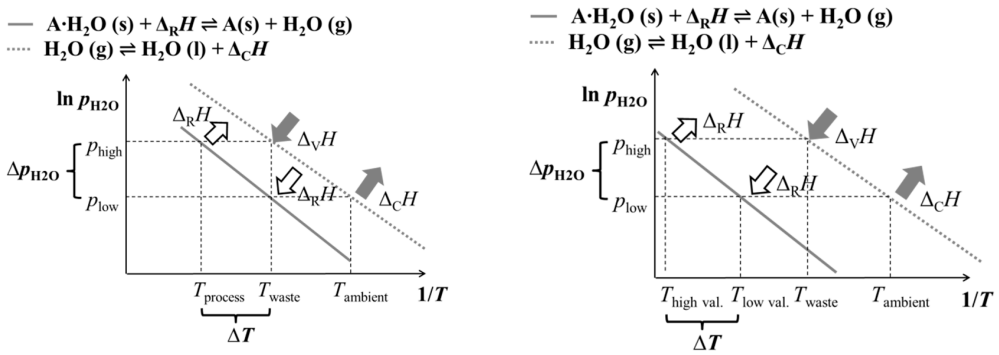

Figure 1. Van't Hoff diagrams of generic water vapor-solid reactions combined with the vapor–liquid equilibrium of the gaseous reactant. Depending on the chosen gas–solid working pair, two modes of operation are possible: (**a**) thermal upgrade of low temperature waste heat (T_{waste} to $T_{process}$) and (**b**) thermal upgrade of high-temperature process heat ($T_{low\ val.}$ to $T_{high\ val.}$) driven by low-temperature waste heat (operation concept of this work).

With this approach, we are able to re-use low-temperature waste heat as a driving source for high-temperature heat pump processes. Depending on the chosen gas–solid working pair, the operating temperatures of the heat pump process can be adapted to a specific application.

In a first study, we identified the hydration and dehydration reaction of strontium bromide ($SrBr_2$) as a potential candidate for thermochemical heat transformation in the temperature range above 150 °C [10]. The non-toxic inorganic salt forms anhydrous, monohydrate, and hexahydrate phases and, prior to our study, it has been discussed in literature exclusively in the context of low-temperature energy storage for seasonal storage applications [11,12]. For achieving low temperatures required in seasonal storage applications, the chemical reaction is limited to the phase change from the monohydrate phase to the hexahydrate phase, which occurs at temperatures of 50 °C to 80 °C. The reaction temperatures can be increased significantly by limiting the phase change from the anhydrous to the monohydrous phase, which is the focus of our work:

$$SrBr_2{\cdot}H_2O\ (s) + \Delta_R H \rightleftharpoons SrBr_2\ (s) + H_2O\ (g) \quad (1)$$

This reversible gas–solid reaction takes place at temperatures of 150 °C or higher, which is very interesting for industrial heat transformation applications as it exceeds the working range of conventional heat pumps. Although the reaction is chemically reversible and cycle stability was

experimentally demonstrated for 10 dehydration/re-hydration reaction cycles in thermogravimetric analysis (TGA) experiments, a thermal hysteresis of 22 K was reported in TGA measurements conducted at a water vapor partial pressure of 5 kPa [10].

The van't Hoff equation provides a first assumption of the correlation between the vapor pressure and reaction temperature based on the standard molar enthalpy and entropy of reaction:

$$\log(p/p^{+}) = \frac{\Delta_R S}{\mathbf{R}} - \frac{\Delta_R H}{\mathbf{R}T}, \quad (2)$$

with **R** being the universal gas constant, and the reference pressure $p^{+} = 10^3$ hPa. From standard molar enthalpy and entropy of formation given in the NBS Tables [13], the reaction enthalpy and entropy is calculated as $\Delta_R H$ = 71.98 kJ/mol and $\Delta_R S$ = 143.93 J/(mol·K), respectively.

For confirming the $p(T)$-correlation, we developed a method for obtaining data from experiments on a 1 kg scale [14]. In the experimental study, we observed that the exothermic reaction from the anhydrous phase to the monohydrate takes place at around 229 °C when water vapor is supplied at a pressure of 70 kPa. This value is higher than the reaction temperature expected from the van't Hoff Equation (2), which returns a temperature of 217 °C for the same vapor pressure. During the dehydration process at a vapor pressure of 6.5 kPa, a minimum temperature of 190 °C was found. Calculated from Equation (2), this vapor pressure corresponds to a reaction temperature of 159 °C. Evidently, the van't Hoff Equation (2) does not give an exact estimation of the correlation between vapor pressure and reaction temperature. However, this correlation is required for further investigations of the heat transformation operation conditions with the $SrBr_2/H_2O$ working pair, and therefore needs to be experimentally determined.

When opening the reaction chamber after having conducted 11 dehydration/re-hydration cycles with different reaction conditions, we detected agglomeration effects in the bulk. Even though this was observed consistently during the series of experiments, the changes in the bulk structure did not affect the reaction dynamics of the thermochemical reactor. Based on the results of these investigations, we see very high potential in the $SrBr_2/H_2O$ working pair for achieving a thermal upgrade of 50 K or more in a single-stage heat transformation process with only one working pair. Therefore, our current work is focused on the investigation of experimental operation conditions and reaction chamber designs that allow for heat transformation in a temperature range of 180 °C to 250 °C at high thermal powers.

2. Materials and Methods

To charge the storage system, thermal energy is transferred indirectly to the solid bulk material via a heat transfer fluid. In the course of the endothermic chemical reaction, the gaseous reactant escapes from the powder bulk and must be separated from the solid phase: the emerging steam is condensed in a separate heat exchanger in order to keep the pressure low and thus to reach complete reaction turnover. In this work, we focus on the thermal discharge process, which starts when water vapor is introduced into the reaction chamber. The thermal energy released by the subsequent chemical reaction is transferred from the powder bulk to the heat transfer fluid. For vapor generation, we use a tube bundle heat exchanger. In order to calculate the reaction conversion, it is equipped with a level indicator measuring the amount of water being consumed during the chemical reaction.

In general, there are three main processes that affect the thermal performance of a thermochemical reactor: vapor mass transfer into the solid bulk phase, heat transfer from the solid bulk phase to the heat transfer fluid, and the rate of the chemical reaction at the given operation conditions. To qualify how the physical and chemical properties of the reactive material affect the thermal performance of a thermochemical reactor and to quantify these local effects in order to identify potential bottlenecks, we included the relevant physical processes during the chemical reaction in a model based on the finite element method (FEM). For numerical calculations, we used solvers from the Comsol Multiphysics® simulation software (Stockholm, Sweden). The validity of the simulation studies is verified by comparison with experimental data from a packed bed thermochemical reactor.

For the validation reactor, a rectangular reaction chamber configuration with indirect heat transfer was chosen. The heat exchanger consisted of two single-embossed pillow plates that were mounted back to back and were equally flowed through by heat transfer fluid (HTF, Purity™ FG Heat Transfer Fluid (Petro-Canada Lubricants Inc., Mississauga, Ontario, Kanada)) at a constant rate of 2 kg/min. The heat exchanger plates formed a 290 mm × 225mm × 20 mm volume filled with 1,050 g of $SrBr_2 \cdot H_2O$ (resulting packed bed height: 205 mm). From the top and the bottom of the reaction chamber, water vapor was introduced into the reactive bulk. Metal filters with a mesh size of 5 µm kept the packed bed in position and minimized undesired release of powder into the pipework of the test setup. The thermochemical reactor was equipped with a pressure sensor and several temperature probes that monitored the solid bulk's temperature at different positions within the fixed bed. During the experiment, the temperature of the heat transfer fluid was kept at a constant value. A schematic drawing of the setup is depicted in Figure 2.

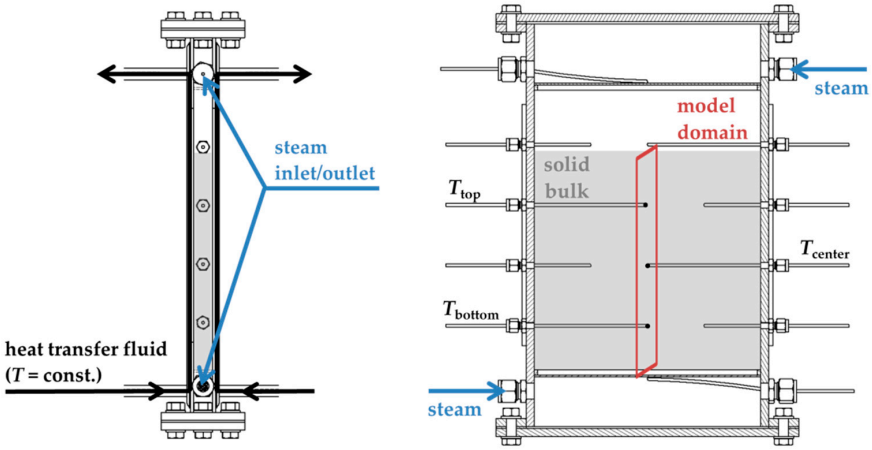

Figure 2. Schematic reactor geometry used for both modelling as well as experimental studies: (**a**) side view and (**b**) front view.

As 2D-model domain, we chose a cross-section through the center of the solid bulk volume. For model implementation, the solid phase was assumed to be a homogenous porous medium. Material properties were assessed by the means of literature data or own measurements and calculations. A summary is given in Table 1.

Table 1. Chemical and physical properties of the $SrBr_2/H_2O$ reaction system.

Category	Parameter	Value	Reference
solid properties	density $SrBr_2$	4216 kg/m^3	literature data [15]
	density $SrBr_2 \cdot H_2O$	3911 kg/m^3	linear interpolation between $SrBr_2$ and $SrBr_2 \cdot 6H_2O$ densities from [15]
	heat capacity $SrBr_2$	75.35 J/(mol·K)	literature data [13]
	heat capacity $SrBr_2 \cdot H_2O$	120.9 J/(mol·K)	literature data [13]
bulk properties ($SrBr_2$ and $SrBr_2 \cdot H_2O$)	bulk porosity ($SrBr_2 \cdot H_2O$)	0.71	experimentally determined for this specific reactor setup
	permeability	$1 \cdot 10^{-10}$ m^2	literature data on $SrBr_2 \cdot H_2O$ [16]
	thermal conductivity λ_{eff}	0.2–0.6 W/(m·K)	assumption based on data on $SrBr_2 \cdot H_2O$ [16]
hydration reaction ($SrBr_2$ to $SrBr_2 \cdot H_2O$)	enthalpy of reaction $\Delta_R H$	71.98 kJ/mol	calculated from literature data on enthalpy of formation [13]
	entropy of reaction $\Delta_R S$	143.93 J/(mol·K)	calculated from literature data on entropy of formation [13]
	effective rate coefficient k_{eff}	$1.6 \cdot 10^{-3}$ 1/s	fit to experimental data from isothermal thermogravimetric analysis (TGA) measurements at 68.8 kPa (unpublished)
	pressure term exponent n	2	

Movement of the solid is neglected, and the porosity is set to a constant value during the reaction. Furthermore, a change in bulk volume or bulk permeability is not yet considered. The gas phase, which consists of pure water vapor with ideal gas properties, penetrates the porous media according to Darcy's law. Local thermal equilibrium is assumed between the gas and the solid phase. As the temperature differences within the observed volume are very small, heat radiation does not play a significant role and is therefore neglected.

Boundary conditions concerning heat and mass transfer in the relevant model domain are depicted in Figure 3. It is assumed that the overall heat transfer coefficient $k_{\text{solid-HTF}}$ from the powder bed to the heat transfer fluid is determined by the heat transfer coefficient on the HTF side of the pillow plate heat exchanger. This value is calculated from the correlations on forced convection in planar gaps given in the VDI Heat Atlas [17] for laminar fluid flow. Assuming the pillow plates as planar gap with 1.5 mm gap width and a HTF flow rate of 2 kg/min result in $k_{\text{solid-HTF}}$ = 365 W/(m^2·K).

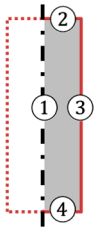

① $\vec{n} \cdot \nabla p = \vec{n} \cdot \nabla \rho_{\text{solid}} = \vec{n} \cdot \vec{v} = \vec{n} \cdot \nabla T = 0$

②, ④ $p = p_{\text{vapor}};\ \vec{n} \cdot \nabla \rho_{\text{solid}} = \vec{n} \cdot \nabla T = 0$

③ $\vec{n} \cdot \nabla \rho_{\text{solid}} = \vec{n} \cdot \vec{v} = 0$

$\vec{n} \cdot (-\lambda_{\text{eff}} \nabla \text{T}) = k_{\text{solid-HTF}} \, (T - T_{\text{HTF}})$

Figure 3. Boundary conditions for heat and mass transfer in the 2D model domain (see Figure 2) with $\vec{v}$ being the Darcy flux and $\vec{n}$ the normal vector.

The exothermic hydration reaction is implemented as a heat source with a first order rate law,

$$\frac{\mathrm{d}X}{\mathrm{d}t} = k_{\text{eff}} \cdot (1 - X) \cdot \left(\frac{p}{p_{\text{R,Hyd}}(T)} - 1 \right)^n, \tag{3}$$

with X being the reaction conversion and p the water vapor (partial) pressure. The effective rate coefficient k_{eff} and the pressure term exponent n given in Table 1 were fitted to isothermal TGA experiments (temperature range 186 °C to 212 °C) at a partial vapor pressure of 68.8 kPa.

In these measurements, it is observed that the effective reaction rate decelerates with increasing temperature, as the equilibrium pressure increases with increasing temperature, thus shifting the system closer to the thermodynamic equilibrium. This rate-diminishing effect is modelled by the last term in Equation (3), and generally prevents any thermal runaway. The temperature-dependent water vapor pressure $p_{\text{R,Hyd}}(T)$ of the hydration reaction can be obtained from thermodynamic data on the reaction enthalpy and reaction entropy (van't Hoff line), as described by Equation (2), or from experimental correlations. Extending the reaction rate model to larger temperature and pressure ranges will be part of our future work.

3. Results

We conducted several sets of experiments. Within the series, the vapor pressure and, accordingly, the temperature of the heat transfer fluid varied: as strontium bromide forms a hexahydrate phase ($SrBr_2 \cdot 6H_2O$) at high vapor pressures or low temperatures, respectively, the preheat temperature of the anhydrous solid must be raised for high vapor pressures in order to ensure the exclusive formation of $SrBr_2 \cdot H_2O$. Up to 15 dehydration/re-hydration cycles were performed in a row with one batch of reactive material. Afterwards, the reactor was refilled with a fresh batch of $SrBr_2 \cdot H_2O$. The vapor pressure was varied from 18 kPa up to 145 kPa, and the discharge temperature was set in a range of 132 °C to 210 °C. The maximum temperature measured at the central position in the packed bed during the hydration reaction is plotted against the set vapor pressure in Figure 4. All experiments considered, the highest maximum temperature was 256 °C at 144 kP vapor pressure.

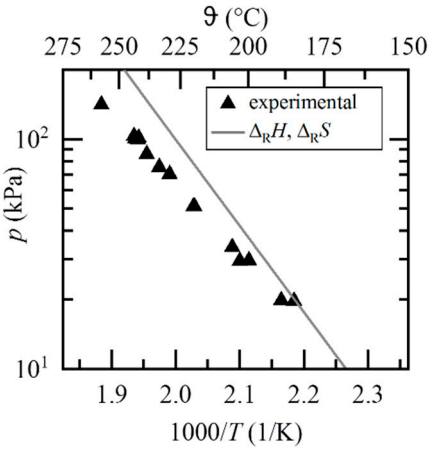

Figure 4. Van't Hoff plot for the hydration reaction: experimental data and correlation based on thermodynamic data ($\Delta_R H$, $\Delta_R S$ calculated from literature data on enthalpy and entropy of formation [13]).

The data points shown in Figure 4 reveal that the measured temperature values clearly exceed the temperatures derived from thermodynamic data, especially for high pressures. For this reason, a linear regression of the experimental data points was calculated to model the temperature dependency of the water vapor pressure $p_{R,Hyd}$ of the hydration reaction in the FEM simulation:

$$\log(p_{R,Hyd}/\text{hPa}) = 8.84 - 3.02 \cdot \frac{10^3}{T/\text{K}}. \quad (4)$$

This correlation was also used in the reaction rate model described in Equation (3).

The simulation study results are compared with the results of the prior described experiments, with the measured pressure curve being defined as input variable for the simulation. In Figure 5a, the temperature progression at different positions within the solid bulk is shown for a discharge temperature of 209.5 °C and a vapor pressure of 70 kPa (corresponding to 90 °C evaporation temperature). The graph includes the results of two simulation studies with varying bulk thermal conductivity λ_{eff}. The increase in temperature indicates that the exothermic reaction is in progress. As the reaction approaches complete conversion to the monohydrate, the temperature in the solid bulk begins to decrease. Evidently, temperature progression in the experimental setup is not homogenous within the bulk phase: at the lowest temperature measuring point (T_{bottom}), a lower maximum temperature is observed. We assume that this effect is caused by macroscopic inhomogeneities within the porous medium, such as cracks, which may affect the temperature measurement. In the simulation study, the temperatures trends at the three positions proceeded identically, which is why only the temperature at the central position of the reactor (T_{sim}) is depicted in Figure 5a. The jumps occurring the temperature curves (e.g., at 1.3 h experimental time) are caused by a sudden increase in pressure due to condensation/evaporation in the setup. The pressure increase leads to a higher reaction temperature in the solid bulk. As the measured pressure curve was used as input parameter for the simulation study, the same effect occurs in the numerical study. In the case of the lower bulk thermal conductivity (λ_{eff} = 0.2 W/(m·K)), maximum temperatures in the simulation were about 7 K lower than in the experiment. In addition, the temperature in the simulation study dropped to its initial value after 3.5 h, whereas in the experiment it was not possible to measure a complete temperature drop even after four hours. In the study with increased bulk thermal conductivity (λ_{eff} = 0.6 W/(m·K)), temperatures dropped to the initial value after two hours.

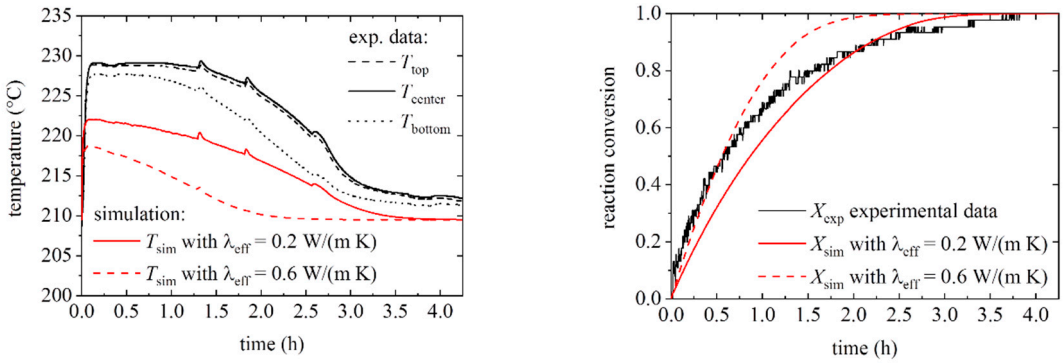

Figure 5. Experimental and simulation results for 209.5 °C discharge temperature and 90 °C evaporation temperature. The simulation study is based on the pressure curve measured in the experiment. (**a**) Temperature profile and (**b**) reaction conversion.

In Figure 5b, the reaction conversion is depicted for both the simulation as well as the experiment, where the turnover is calculated from the fluid level measurement. In the initial study with λ_{eff} = 0.2 W/(m·K), the experimental yield is higher than the simulation result up to a turnover of roughly 85%. Afterwards, the progress of the experimental turnover decelerates for high reaction yields, and full turnover is achieved about 20 min later in the experiment than in the corresponding simulation study. Increasing the thermal conductivity of the bulk phase to λ_{eff} = 0.6 W/(m·K) leads to significantly shorter discharging times.

4. Discussion

Although the model does not reproduce the experiments quantitatively due to the uncertainty of the input parameters (in particular, the parameters of the reaction rate model and macroscopic inhomogeneities), it allows for the qualitative observation and identification of the factors having the greatest influence on the progression of the hydration reaction and thus on the discharge of the storage module.

From the observation that the simulated temperature curves perfectly overlap for the three different positions within the fixed bed, the conclusion can be drawn that mass transport within the bulk material does not lead to a limitation for the given hydration reaction conditions. This is an important finding for the design of suitable reactor geometries. Still, this effect should be further analyzed regarding the lower absolute pressures and gas densities during the charging process of the thermochemical reactor.

The influence of low bulk thermal conductivities on the reaction turnover curve and, hence, the reactor's overall performance was numerically studied. Increasing the effective thermal conductivity from 0.2 to 0.6 W/(m·K) (f.e. by adding highly conductive additives such as aluminum) reduces the total discharging time by 40% in the simulation study (3.5 h versus 2.1 h for 99% reaction conversion). This is equivalent to a 1.7 times higher average thermal power. According to the experimental results of the generic reactor geometry presented in this work, we recommend a maximum heat transport distance of 10 mm for the design of high-power thermochemical reactors based on $SrBr_2/H_2O$. Furthermore, the effective thermal conductivity of the bulk could be increased by adding highly conductive inert additives or by the integration of heat conducting structures.

The FEM simulation developed in this work can be used as design tool for the layout of high-power reactor geometries. We assume that the following modifications of the first model can improve the prediction quality of the simulation: firstly, the mathematical model of the reaction rate over-estimates the rate at higher yields. Therefore, the development of an advanced reaction rate model is a subject of our ongoing work. Secondly, the solid bulk is not a homogenous porous medium; therefore, slower reaction progress can occur locally, which is not considered in the model. Moreover, in further

experimental work, we found that the macroscopic and the microscopic properties of the solid bulk material change considerably due to the chemical reaction: the primary particles agglomerated, which was already observed in the experiments described above, and the overall volume of the porous bulk increased after several dehydration/re-hydration cycles [18]. The observed structural changes could also affect the bulk thermal conductivity and thus have an effect on the long-term thermal performance of the storage reactor.

From the thermodynamic point of view, a discharging temperature of 250 °C is feasible with the reaction system $SrBr_2/H_2O$. To achieve this high reaction temperature, steam must be supplied with a pressure of approx. 140 kPa or higher. This requires waste heat temperatures of at least 110 °C for vapor generation. At the same time, the discharging temperature must not be too low: as strontium bromide forms a hexahydrate phase ($SrBr_2 \cdot 6H_2O$) at high vapor pressures or low temperatures, respectively, the minimum discharge temperature must be raised for high vapor pressures in order to ensure the exclusive formation of $SrBr_2 \cdot H_2O$.

Taking the reaction kinetics into account, a minimal temperature difference of 10 K or more between the reaction temperature and the temperature of the heat transfer fluid could be required in case the chemical reaction decelerates considerably close to the thermodynamic equilibrium. This would significantly decrease the thermal power of the storage reactor, or limit the maximum possible discharge temperature. Quantifying the required temperature difference for high reaction rates is part of our ongoing work.

5. Conclusions

In a previous study based on thermogravimetric experiments performed on a mg scale, we identified strontium bromide ($SrBr_2$) as a promising candidate for thermochemical heat transformation [10]. The work presented here is focused on the investigation of the exothermic hydration reaction from the anhydrous $SrBr_2$ to its monohydrate phase on a 1 kg scale. Our objective is the identification of suitable operation conditions that allow for heat transformation with output temperatures in the range of 180 °C to 250 °C. Our key findings are as follows:

- The working pair $SrBr_2/H_2O$ allows discharging temperatures up to 250 °C when water vapor is supplied at 110 °C (f.e. driven by low-temperature waste heat);
- Vapor mass transfer in the porous bulk phase does not limit the thermal discharging performance in the analyzed reactor setup;
- The low effective thermal conductivity of the fixed reactive bed is a potential bottleneck for high-power thermochemical storage and heat transformation modules.

Based on the experimental results and the conclusions of our simulation studies presented here, we are currently developing a reactor setup that allows for high specific thermal powers, and which is easily scalable for industrial applications. To increase the effective thermal conductivity of the bulk phase, we are using heat conducting structures made from aluminum. Further design considerations include a minimum pressure loss on the vapor side and a reaction chamber design that is robust with respect to changes of the bulk's macroscopic structure. With this design, we expect to achieve specific thermal powers of minimum 0.25 kW per kg of $SrBr_2$. Future work will include investigations with our new test facility, allowing for heat transformation with thermal powers up to 5 kW and output temperatures of up to 320 °C. In particular, quantifying the required temperature difference between the solid's reaction temperature and the discharge temperature, ensuring high reaction rates and, thus, high thermal powers, will be part of our future work.

Author Contributions: All authors contributed to this work by collaboration: conceptualization, experimental investigation, and simulation, J.S.; simulation and validation, J.W.; project supervision, M.L. J.S. is the main author of this manuscript. All authors revised and approved the publication.

Funding: This research was funded by the German Federal Ministry for Economic Affairs and Energy (BMWi, "Bundesministerium für Wirtschaft und Energie"), "TheSan" project (03ET1297A).

Conflicts of Interest: The authors declare no conflict of interest. The funders had no role in the design of the study; in the collection, analyses, or interpretation of data; in the writing of the manuscript; or in the decision to publish the results.

Nomenclature

The following abbreviations are used in this manuscript:

eff	effective
exp	experimental
FEM	finite element method
g	gas
H_2O	water
HTF	heat transfer fluid
Hyd	hydration
l	liquid
R	reaction
s	solid
sim	simulation
$SrBr_2$	strontium bromide
TGA	thermogravimetric analysis

The following Latin variables are used:

$\Delta_C H$	standard molar enthalpy of condensation, J/mol
$\Delta_R H$	standard molar enthalpy of reaction, J/mol
$\Delta_V H$	standard molar enthalpy of evaporation, J/mol
$\Delta_R S$	standard molar entropy of reaction, J/(mol·K)
k_{eff}	effective reaction rate coefficient, 1/s
$k_{solid-HTF}$	Solid-to-HTF heat transfer coefficient, W/(m^2·K)
n	pressure term exponent
p	water vapor pressure, Pa
p^+	reference pressure, 10^3 hPa
R	universal gas constant, 8.3145 J/(mol·K)
T	temperature, K
X	yield of reaction

The following Greek variables are used:

λ_{eff}	thermal conductivity, W/(m·K)
ρ	density, kg/m^3

References

1. Aydin, D.; Casey, S.P.; Riffat, S. The latest advancements on thermochemical heat storage systems. *Renew. Sustain. Energy Rev.* **2015**, *41*, 356–367. [CrossRef]
2. Wongsuwan, W.; Kumar, S.; Neveu, P.; Meunier, F. A review of chemical heat pump technology and applications. *Appl. Therm. Eng.* **2001**, *21*, 1489–1519. [CrossRef]
3. Cot-Gores, J.; Castell, A.; Cabeza, L.F. Thermochemical energy storage and conversion: A-state-of-the-art review of the experimental research under practical conditions. *Renew. Sustain. Energy Rev.* **2012**, *16*, 5207–5224. [CrossRef]
4. Spoelstra, S.; Haije, W.G.; Dijkstra, J.W. Techno-economic feasibility of high-temperature high-lift chemical heat pumps for upgrading industrial waste heat. *Appl. Therm. Eng.* **2002**, *22*, 1619–1630. [CrossRef]
5. Chan, C.W.; Ling-Chin, J.; Roskilly, A.P. A review of chemical heat pumps, thermodynamic cycles and thermal energy storage technologies for low grade heat utilisation. *Appl. Therm. Eng.* **2013**, *50*, 1257–1273. [CrossRef]
6. Wu, S.; Li, T.X.; Yan, T.; Wang, R.Z. Experimental investigation on a novel solid-gas thermochemical sorption heat transformer for energy upgrade with a large temperature lift. *Energy Convers. Manag.* **2017**, *148*, 330–338. [CrossRef]

7. Willers, E.; Groll, M. Two-stage metal hydride heat transformer. *Int. J. Hydrogen Energy* **1999**, *24*, 269–276. [CrossRef]
8. Haije, W.G.; Veldhuis, J.B.J.; Smeding, S.F.; Grisel, R.J.H. Solid/vapour sorption heat transformer: Design and performance. *Appl. Therm. Eng.* **2007**, *27*, 1371–1376. [CrossRef]
9. Yu, Y.; Zhang, P.; Wu, J.; Wang, R. Energy upgrading by solid–gas reaction heat transformer: A critical review. *Renew. Sustain. Energy Rev.* **2008**, *12*, 1302–1324. [CrossRef]
10. Richter, M.; Habermann, E.-M.; Siebecke, E.; Linder, M. A systematic screening of salt hydrates as materials for a thermochemical heat transformer. *Thermochim. Acta* **2017**, *659*, 136–150. [CrossRef]
11. Mauran, S.; Lahmidi, H.; Goetz, V. Solar heating and cooling by a thermochemical process. First experiments of a prototype storing 60 kW h by a solid/gas reaction. *Sol. Energy* **2008**, *82*, 623–636. [CrossRef]
12. Marias, F.; Neveu, P.; Tanguy, G.; Papillon, P. Thermodynamic analysis and experimental study of solid/gas reactor operating in open mode. *Energy* **2014**, *66*, 757–765. [CrossRef]
13. Wagman, D.D.; Evans, W.H.; Parker, V.B.; Schumm, R.H.; Halow, I.; Bailey, S.M.; Churney, K.L.; Nuttal, R.L. The NBS Tables of Chemical Thermodynamic Properties. Selected Values for Inorganic and C1 and C2 Organic Substances in SI Units. *J. Phys. Chem. Ref. Data* **1982**, *18*, 1807–1812. [CrossRef]
14. Stengler, J.; Ascher, T.; Linder, M. High temperature thermochemical heat transformation based on SrBr2. In Proceedings of the 12th IEA Heat Pump Conference, Rotterdam, The Netherlands, 15–18 May 2017.
15. Perry, D.L. *Handbook of Inorganic Compounds*, 2nd ed.; Taylor & Francis: Boca Raton, FL, USA, 2011; ISBN 1439814619.
16. Michel, B.; Neveu, P.; Mazet, N. Comparison of closed and open thermochemical processes, for long-term thermal energy storage applications. *Energy* **2014**, *72*, 702–716. [CrossRef]
17. Stephan, P.; Kabelac, S.; Kind, M.; Mewes, D.; Schaber, K.; Wetzel, Th. (Eds.) *VDI-Wärmeatlas*, 11th ed.; Springer: Berlin/Heidelberg, Germany, 2013; ISBN 978-3-642-19981-3.
18. Stengler, J.; Gollsch, M.; Weiss, J.; Linder, M. Porous media for thermochemical energy storage: Experimental investigation on structural changes of reactive materials. Presented at the InterPore Conference 2018, New Orleans, LA, USA, 14–17 May 2018.